Proceedings of the 7th International Conference on HydroScience and Engineering

Philadelphia, USA September 10-13, 2006 (ICHE 2006)

ISBN: 0977447405

Drexel University

College of Engineering

LARGE EDDY SIMULATION OF FLOW PAST FREE SURFACE PIERCING CIRCULAR CYLINDERS

Guangxu Yu[1], Eldad Avital[2] and John Williams[3]

ABSTRACT

Flows past a free surface piercing cylinder are studied numerically by large eddy simulation (LES) at Froude numbers up to Fr_D=2.0 and Reynolds numbers up to Re_D=1.10^5. A two-phase FCT-VOF method is employed to simulate the air-water interface. The effects of the free surface on vortex structure in the near wake are particularly investigated. The loadings on the cylinder at various Reynolds and Froude numbers are also studied.

Computation results show the free surface inhibits the vortex generation in the near wake, and this effect is stronger at higher Froude numbers, nevertheless, it is attenuated as the Reynolds number increases. It is also found that the strong three dimensionality in the near wake at higher Froude numbers affects the force distribution dramatically along the cylinder, whereas variation in the Reynolds number has no significant effect.

1. INTRODUCTION

Flow past free surface piercing cylinders is of particular relevance to offshore structures and underwater vessels. The flow is known to show different complex structures in the vicinity of the cylinder, a bow wave appears in front of it which then spills over the cylinder to generate the near wake. The bow wave can break up and develop into a fountain in front of the cylinder at higher flow velocities. A Kelvin surface wake is generated behind the cylinder, which fans out to the far distance rear. The detailed hydrodynamics affecting this process are poorly understood and studies either by experimental tests or numerical simulations are rare. Wickramasinghe and Wilkinson (1997) explored the possibilities of different methods, including practical tests, computational modeling and theoretical analysis, that might be used for the study of the flow around a submarine mast. Inoue et al. (1993) experimentally investigated cases with a vertical surface piercing cylinder at two Froude numbers, Fr_D=0.8, and 1.0. Most numerical simulations by now have either been restricted to inviscid free surface flows for example in Ferrant and Guillern (1998) or neglected the free surface

[1] Research Assistant, Department of Engineering, Queen Mary College, University of London, London, E1 4NS, UK (g.yu @qmul.ac.uk)
[2] Reader, Department of Engineering, Queen Mary College, University of London, London, E1 4NS, UK (e.avital@qmul.ac.uk)
[3] Professor, Department of Engineering, Queen Mary College, University of London, London, E1 4NS, UK (j.j.r.williams@qmul.ac.uk)

waves, such as in Tseng and Song (2000). Only recently, LES results were produced by Kawamura et al. (2002) for $Fr_D \leqslant 0.8$ and sub-critical Reynolds number of $Re_D=2.7.10^4$.

In this work, flows at various Froude numbers up to $Fr_D=2.0$ and Reynolds numbers up to $Re_D=1.10^5$ are studied. The primary objective is to investigate the effects of the free surface on flow structures in the near wake, and the force distribution along the cylinder.

2. METHOD

The flow is taken as incompressible consisting of two phases, water and air, with a clearly determined moving interface surface separating them. Both phase flows are governed by the following two-phase non-dimensional equations which are then transformed into cylindrical coordinates:

$$\frac{\partial u_i}{\partial t}+\frac{\partial u_i u_j}{\partial x_j}=-\frac{1}{\rho}\frac{\partial p}{\partial x_i}+\frac{1}{Fr_D^2}g_i+\frac{1}{\rho}\frac{\partial}{\partial x_j}\left[\left(\frac{\mu}{\mathrm{Re}_D}+\rho\nu_t\right)\left(\frac{\partial u_i}{\partial x_j}+\frac{\partial u_j}{\partial x_i}\right)\right] \tag{1}$$

$$\frac{\partial c}{\partial t}+\frac{\partial u_i c}{\partial x_i}=0 \tag{2}$$

$$\rho=c+(1-c)\frac{\rho_g}{\rho_l},\ \mu=c+(1-c)\frac{\mu_g}{\mu_l} \tag{3}$$

$$\frac{\partial u_i}{\partial x_i}=0 \tag{4}$$

where u_i and p are the filtered velocity and pressure, x_i is the coordinate and t is the time, $g_i=(0,0,-1)$ is a unit vector pointing in the direction of gravity. c is a fractional volume scalar that is 1 when the computational cell is full of water and 0 if occupied by air. ρ_g ρ_l and μ_g μ_l represent the density and dynamic viscosity of air and water respectively. The dimensionless parameters are Froude number, $Fr_D=U/\sqrt{gD}$, and Reynolds number of water, $\mathrm{Re}_D=\rho_l UD/\mu_l$ where U and D are the water inflow velocity and the cylinder diameter, g is the gravitational acceleration.

The Smagorinsky model with the Van Driest wall damping function is used to model subgrid small scales, the eddy viscosity is given by

$$\nu_t=C_s^2\Delta^2(1-\exp(-y^+/A)^3)\sqrt{2S_{ij}S_{ij}} \tag{5}$$

As stated in Piomelli et al. (1988), for wake and jet flows the optimum value of Smagorinsky's constant C_s is around 0.2 which was also the value used by Kawamura et al. (2002) to study the interaction between the turbulent wake and the free surface. For Case 1 (in Table 1) the authors confirmed that when taking into account the free surface, $C_s=0.2$ gave the closest prediction of mean drag coefficient to the experimental value of 1.2 in Szepessy et al. (1992) for the same configuration but neglecting the free surface. Δ is the cubic root of the volume of a computational cell, $S_{ij}=\frac{1}{2}\left(\frac{\partial u_i}{\partial x_j}+\frac{\partial u_j}{\partial x_i}\right)$ is the rate of strain tensor and y^+ is the non-dimensional distance from the wall defined by $y^+=\frac{u_\tau y}{\nu}$, where μ_τ is the wall shear velocity and

$\nu = c + (1-c)(\mu_g / \mu_l)/(\rho_g / \rho_l)$, $A = 25$ is the Van Driest constant. The value of y^+ of the first point off the cylinder varies in azimuthal direction due to the different wall shear velocities in this direction. The average value of y^+ of the first point off the cylinder is listed in Table 1.

The spatial discretization is based on the finite volume approach applied for a staggered grid, the QUICK scheme is used for the convection term and a second order central scheme for the diffusion term. Breuer (1998) investigated the effects of numerical schemes for the convection term and found the QUICK scheme is not very suitable for flows past an infinite circular cylinder, instead a second order central scheme gives a better agreement with the experiment data. Nevertheless, this scheme failed to converge when applied to free surface flows past a piercing circular cylinder and it is probably due to the free surface deformation and the large density ratio of water and air. Equation (1) is solved by the projection method and marched in time by a second order Runge-Kutta (RK) scheme; the Poisson equation for pressure resulting from the projection method is solved using the Preconditioned Bi-Conjugate Gradient Stabilized (PBCGSTAB) method along with a polynomial pre-conditioner. Free surface motion is modeled using an air-water two-phase volume of fluid (VOF) model with the air initially on top of the water by equation (2) which is solved based on flux corrected transport (FCT) method of Rudman (1997). The coupling of the equation (1) and (2) at each RK stage is illustrated as follows:

1. Calculate the value of c at sub-time level $n+1$ using FCT method

$$c^{n+1} = c^n - \delta t \left(\frac{\partial u_i c}{\partial x_i} \right)^n \tag{6}$$

2. Find the densities and viscosities at the sub-time level $n+1$

$$\rho^{n+1} = c^{n+1} + (1-c^{n+1})\frac{\rho_g}{\rho_l},\ \mu^{n+1} = c^{n+1} + (1-c^{n+1})\frac{\mu_g}{\mu_l} \tag{7}$$

3. Estimate intermediate values of velocities at the sub-time level $n+1$

$$\left(u^{n+1}\right)^* = u^n - \delta t H^n,\ H = -\frac{\partial u_i u_j}{\partial x_j} + \frac{1}{Fr_D^2} g_i + \frac{1}{\rho}\frac{\partial}{\partial x_j}\left[\left(\frac{\mu}{\mathrm{Re}_D} + \rho \nu_t \right)\left(\frac{\partial u_i}{\partial x_j} + \frac{\partial u_j}{\partial x_i} \right) \right] \tag{8}$$

4. Solve the Possion equation for pressure at the sub-time level $n+1$

$$\frac{\partial}{\partial x_i}\left(u^{n+1}\right)^* = \frac{\partial}{\partial x_i}\left(\frac{\delta t}{\rho^{n+1}} \left(\frac{\partial p}{\partial x_i} \right)^{n+1} \right) \tag{9}$$

5. Update the velocities (divergence-free) at the sub-time level $n+1$

$$u^{n+1} = \left(u^{n+1}\right)^* - \frac{\delta t}{\rho^{n+1}} \left(\frac{\partial p}{\partial x_i} \right)^{n+1} \tag{10}$$

A body fitted cylindrical grid is used to capture the form of the cylinder. The computational domain is composed of inflow & outflow regions along with a buffer zone ringed around the computational domain (see Fig.1). The domain size for the cases studied and the corresponding grid points are shown in Table 1.

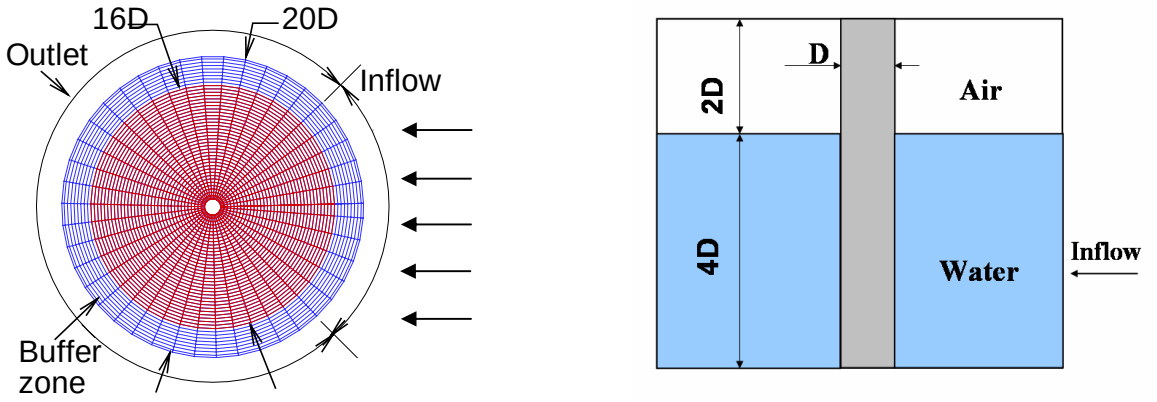

Figure 1: Schematic description of the cylindrical co-ordinates and the configurations of the computational domain. The inflow region covers an arc of $90^{0.}$

For all the simulations in this study, the still water height is 4D. A non-slip wall condition is imposed on the cylinder surface for the velocity. The free stream water inflow velocity is perturbed by a small amplitude sinusoidal wave to increase the inlet turbulence, the air is taken as stationary; at outlet a zero gradient velocity condition is applied in radial direction along with a buffer zone in which the computation scheme for the convection term is relaxed from the QUICK to a first order upwind scheme to dampen reflections. At the bottom (water side) of the computation domain a free slip velocity condition is adopted, which means no horseshoe vortex develops there; the same free slip condition is also applied on the top (air side). Pressure is set to zero on the top of the domain, whilst a zero gradient pressure is applied at boundaries elsewhere. Due to the high density ratio of water and air, a δ-function interpolation is used to smoothen the density in the vicinity of the interface.

3. RESULTS AND DISCUSSION

Table 1 summarizes the cases studied in this paper.

Table 1: Flows simulated and the size of the computation domain employed

	Re_D	Fr_D	Domain (Radius x Height)	Grid size (azimuthal x radial x height)	$< y^+ >$
Case 1	27000	0.8	10D x 6D	129 x 129 x 99	~35.8
Case 2	100000	0.8	10D x 6D	129 x 129 x 99	~74.2
Case 3	27000	2.0	12D x 8D	129 x 161 x 131	~33.6

3.1 Free Surface Effect on Flow Structures in the Near Wake

Figure 2 shows the deformation of air-water interface for Case 1 in Table 1, a bow wave in front of the cylinder is generated and a Kelvin wake is also observed after the cylinder.

It has been found that the free surface inhibits the vortex generation in the near wake, as a result the lift oscillation also bears this influence. As shown in Figure 3, a vortex street is observed below the midplane (2D above the bed), the corresponding lift oscillation is characterized by a dominant mode of $St_D = 0.23$, where $St_D = fD/U$ and f is the oscillation frequency; as the free

surface is approached, no dominant frequency exists and the oscillation intensity is reduced. Oscillations with smaller frequencies develop and become completely random.

Figure 4 presents the effects of the free surface on the time-averaged vorticity magnitude $<\omega>$ and Reynolds stress $<u'v'>$. There is no significant difference in the time-averaged vorticity magnitude below the midplane, the transverse spatial distance of each shear layer in the near wake is very narrow indicating a very high vorticity gradient of the shear layer, moreover, each layer is drawn towards the plane of symmetry of the base region; near the free surface each layer is deflected away from the symmetric plane, and the vorticity in the shear layer is reduced. As described by Gerrard (1966), vortex shedding occurs when the vorticity in the shear layer is strong enough to draw the opposing vortex across the wake to cut off further supply of vorticity from the shear layer. Below the midplane, free surface effect on the vorticity is very weak and a regular vortex street is observed; near the free surface, due to the reduced vorticity in the shear layer by the free surface effect, no vortex shedding forms.

It is also observed that the free surface reduces $<u'v'>$ in the near wake, high concentration centers of $<u'v'>$ are displaced further down stream as the free surface is approached. Furthermore, in the wake below the midplane an additional but weaker concentration pair occurs close to the base of the cylinder, this overall form of the Reynolds stress pattern qualitatively agrees with the experimental observation in the near wake of a cylinder with a larger span wise extent as presented by Mittal and Balachandar (1995). It should be noted that the lack of complete anti-symmetry of $<u'v'>$ is due to a shorter time interval for the statistics or probably a lack of convergence of the calculations in the pressure solver.

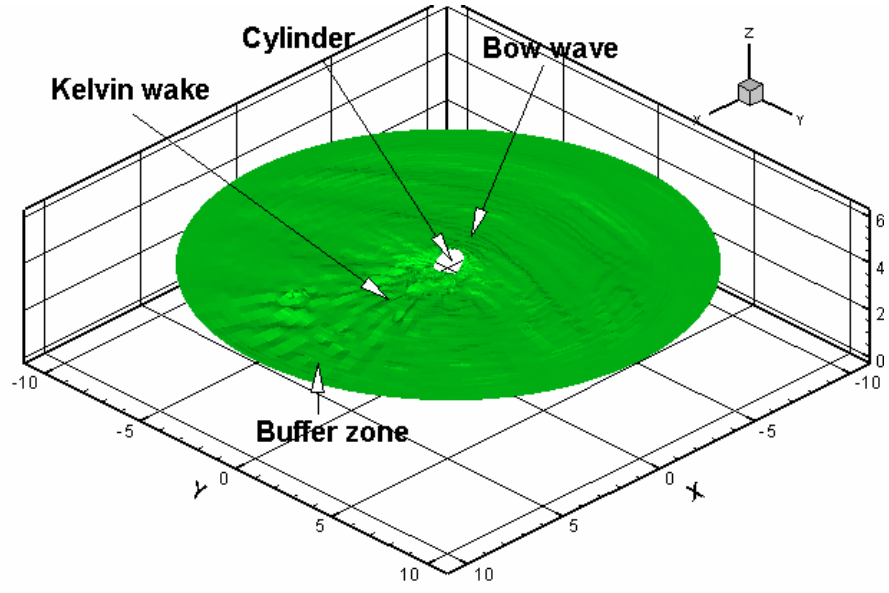

Figure 2: Instantaneous evolution of the interface surface, $Re_D=22.7.10^4$, $Fr_D=0.8$.

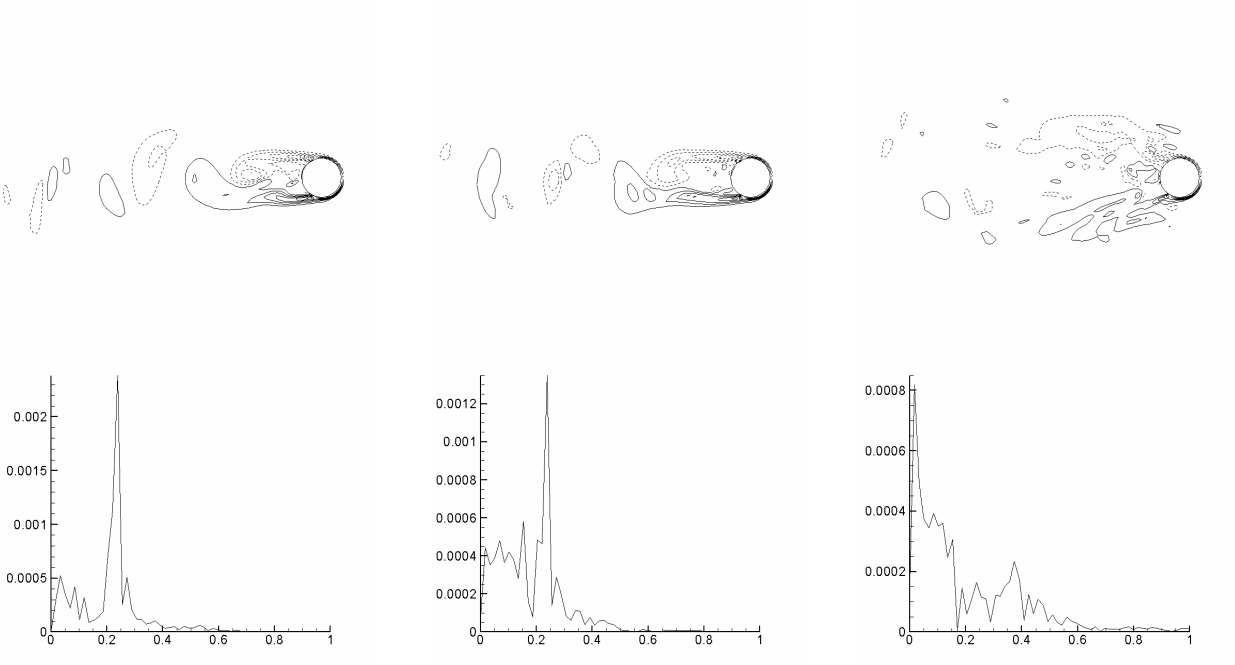

Figure 3: Contours of instantaneous vorticity magnitude (top row) and power spectral density of the lift (bottom row) for case 1 on the plane adjacent to the bed (left), at the midplane (middle) and near the free surface (right), the horizontal axis is the St_D number

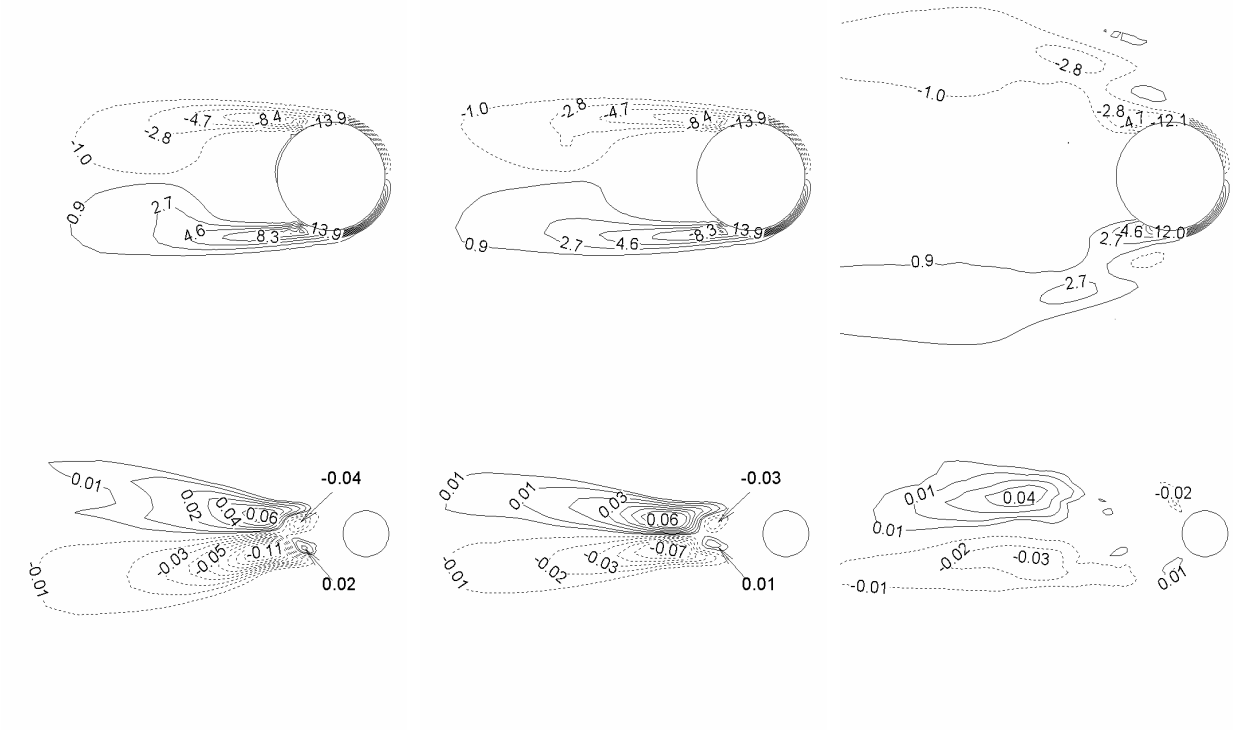

Figure 4: Contours of time-averaged magnitude vorticity (top row) and Reynolds stress $< u'v' >$ (bottom row) for case 1 on the plane adjacent to the bed (left), at the midplane (middle) and near the free surface (right)

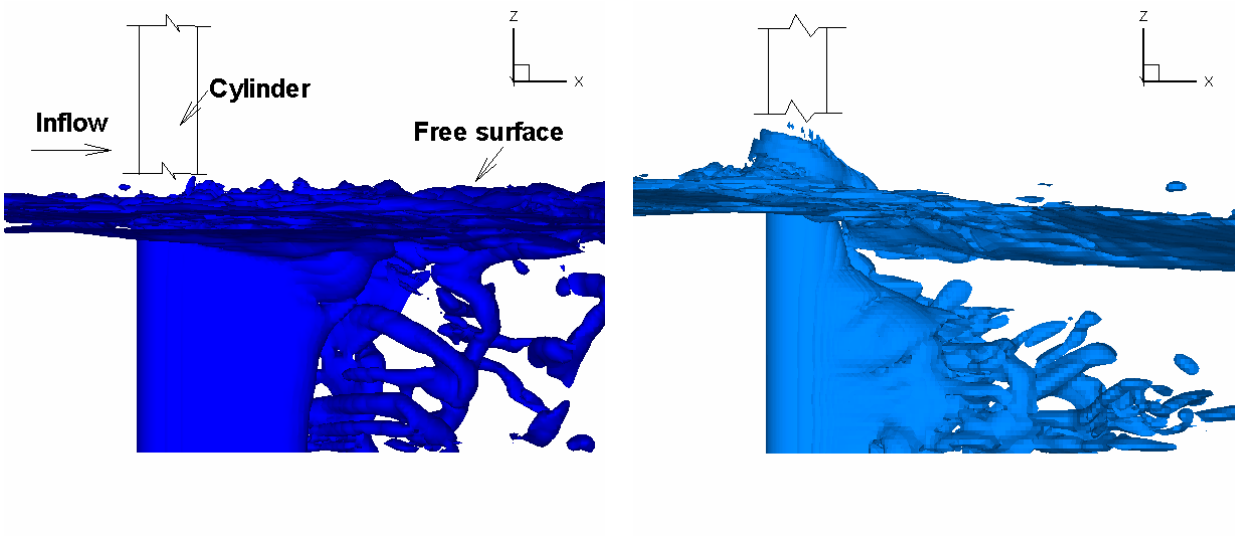

Figure 5: Side-view of instantaneous vortex structure in the near wake at Re_D=2.7.10^4; Fr_D=0.8 (left) and Fr_D=2.0 (right), the view is taken on the plane cross the cylinder centre in the inflow direction

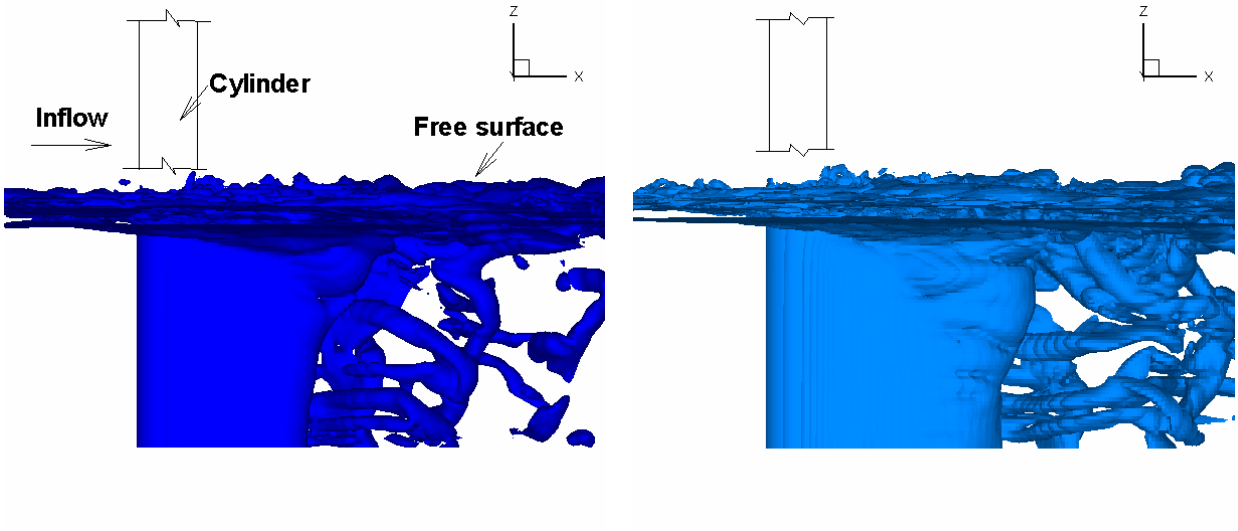

Figure 6: Side-view of instantaneous vortex structure in the near wake at Fr_D=0.8; Re_D=2.7.10^4 (left) and Re_D=1.0.10^5 (right), the view is taken on the plane cross the cylinder centre in the inflow direction

By employing the λ-criterion defined by Jeong and Hussain (1995), three-dimensional coherent vortex structures can be identified in the near wake.

Figure 5 shows the instantaneous vortex structure for flows at the same Reynolds number but with two different Froude numbers, the iso-surface is plotted at $\lambda = 3.3$. At Froude number of 0.8, fewer effects of the free surface can be felt in the deep wake resulting in a region where 2D flow features dominate, vortex tubes lie on horizontal planes; above the midplane the shed vortex tubes slant and near the free surface they re-attach to the free surface exhibiting a strong 3D feature of the flow. At Fr_D=2.0, the free surface effect has propagated throughout the wake, and no regular vortex shedding is observed; vortices with less intensity dominate the region well below the free surface.

Vortex structures for flows at the same Froude number but two different Reynolds numbers are shown in Figure 6 with the iso-surface plotted at $\lambda = 3.3$. It is observed that at a higher Reynolds

number, Re_D=1.0.10^5, the 2D flow feature exists up to a position closer to the free surface than that at a lower Reynolds number, Re_D=2.7.10^4, which implies that flows at a higher Reynolds number can swamp the free surface effect on the vortex structure in the near wake. This feature can also be demonstrated by doing spectrum analysis on lift as shown in Figure 7. The dominant St_D number of lift oscillation adjacent to bed at Re_D=1.0.10^5 is 0.2 which is consistent with the typical value of a 2D flow past a horizontal cylinder, whereas it is 0.23 for Re_D=2.7.10^4 indicating the free surface effect can still be sensed even near the bed. It is also noted that the oscillation intensity at Re_D=1.0.10^5 is less reduced, which again verifies the observation that flows at a higher Reynolds number inhibit the free surface effect. With the value of λ at which the iso-surface is plotted in both Figure 6 and 5, there are no vertex structures observed in front of the cylinder.

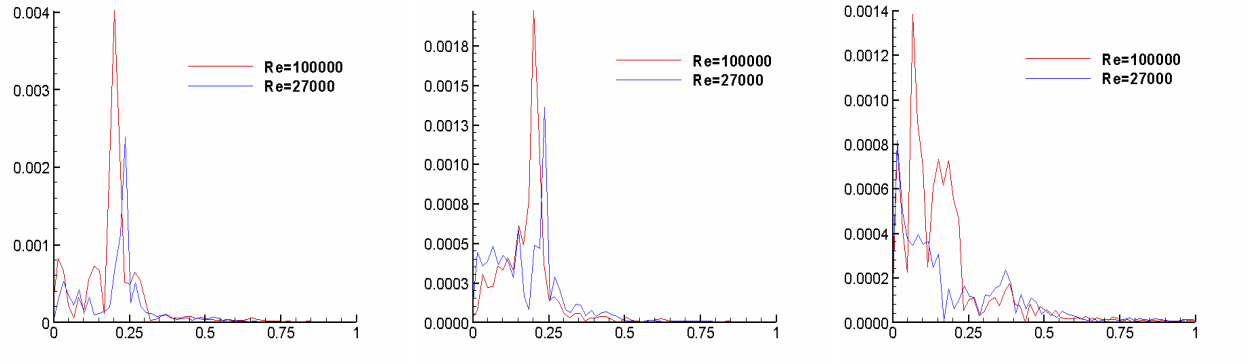

Figure 7: Power spectral density of the lift at Fr_D=0.8, on the plane adjacent to the bed (left), at the midplane (middle) and near the free surface (right) , the horizontal axis is the St_D number

3.2 Free Surface Effect on Loading Distribution along the Cylinder

It has been found that for the same water height of 4D and Froude number, variation in the Reynolds number has only a small effect on the distribution of the sectional mean drag and r.m.s. lift along the cylinder (see Figure 8 left); on the other hand, the Froude number affects strongly the loadings on the cylinder for flows at a constant Reynolds number. At a higher Froude number, Fr_D=2.0, in the region just below the free surface there is a huge increase of both the mean drag and r.m.s. lift (see Figure 8 right).

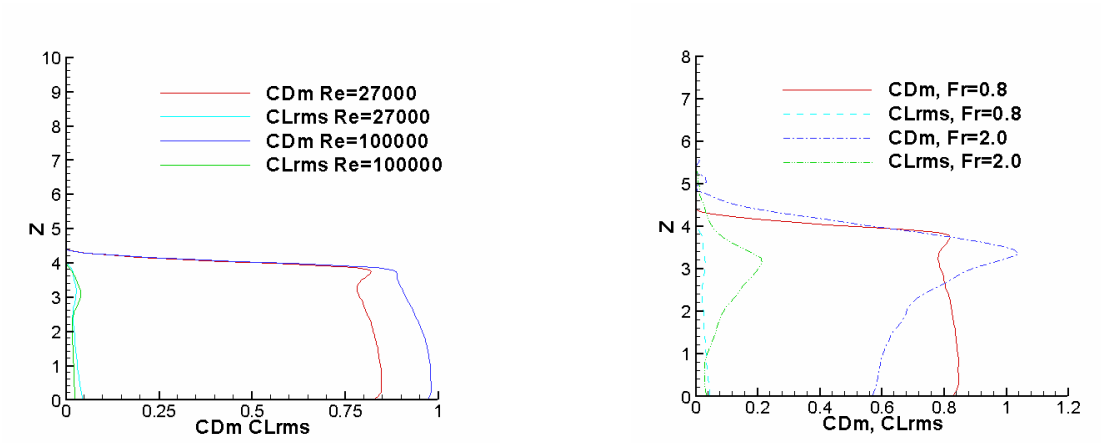

Figure 8: Sectional mean drag coefficient (CDm) and r.m.s. lift coefficient (CLrms) at Fr_D=0.8 for various Reynolds numbers (left) and at Re_D=2.7.10^4, Fr_D=0.8, 2.0 (right). The still water height is 4D for all the cases, and the vertical axis Z represents the cylinder height.

4. CONSUSION

This study has shown that the free surface attenuates the vortex generation in the near wake and, as a result, reduces the vorticity and vortex shedding. As the Froude number increases, the vorticity in the near wake is further decreased, and the vortex shedding is no longer a dominant feature. As the Reynolds number increases, the free surface effect on the flow structure is inhibited. The force distribution along the cylinder depends dramatically on the Froude numbers, whereas variation of the Reynolds number has no significant effects.

ACKNOWLEDGEMENTS

The support of the EPSRC grant GR/S46239/1 and the UK Turbulence Consortium for providing computing time are gratefully acknowledged.

REFERENCES

Breuer, M. (1998). “Large Eddy Simulation of the Subcritical Flow past a Circular Cylinder: Numerical and Modeling Aspects”, Int. J. Num. Meth. in Fluids, 28, pp. 1281-1302.

Ferrant, P. and Guillern, P. E. (1998). “Interaction of Second Order Wave Packets with a Vertical Cylinder”, Proc. 8th Int. Offshore Polar Eng. Conf, Vol. III, pp. 340-347.

Gerrard, J. H. (1966). “The Mechanics of the Formation region of vortices behind bluff bodies”, J. Fluid Mech., 25, pp. 401-413.

Inoue, M., Baba, N. and Himeno, Y. (1993). “Experimental and Numerical Study of Viscous Flow Field around an Advancing Vertical Circular Cylinder Piercing a Free Furface”, J. Kansai Soc. Nava Archit. Japan, 220, pp. 57-64.

Jeong, J., Hussain, F. (1995). “On the Identification of a Vortex”, J. Fluid Mech., 285, pp. 69-94.

Kawamura, T., Mayer, S., Garapon, A. and Sorensen, L. (2002). “Large Eddy Simulation of a Flow past a Free Surface Piercing Circular Cylinder”, J. of Fluids Engineering, 124, pp. 91-101.

Mittal, R., Balachandar, S. (1995). “Effect of Three-dimensionality on the Lift and Drag of Nominally Two-dimensional Cylinders”, Phys. Fluids, 7 (8), pp.1841-1865.

Piomelli, U., Moin, P., and Ferziger, J. H. (1988). “Model Consistency in Large Eddy Simulation of Turbulent Channel Flows”, Phys. Fluids A, 31, pp.1884-1891.

Rudman, M. (1997). “Volume-tracking Methods for Interfacial Flow Calculations”, Int. J. Num. Meth. Fluids, 24, pp. 671-691.

Tseng, M. H., Yen, C. L. and Song, C. C. S. (2000). “Computation of Three–dimensional Flow Around Square and Circular Piers”, Int. J. Num. Meth. Fluids, 34, pp. 207-227.

Wickramasinghe, D. and Wilkinson, R.H. (1997). Wakes and Waves Generated by Surface Piercing Cylinders, DRA study Report EX 3545.